Journal of Marine Science and Technology

Volume 26 | Issue 4 Article 8

MORPHOLOGICAL CHARACTERISTICS OF TIDAL INLETS SUBJECT TO A SHORT TERM TYPHOON EVENT: A CASE STUDY IN LANYAN RIVER ESTUARY

Hsing-Yu Wang
Department of Harbor and River Engineering, National Taiwan Ocean University, Keelung, Taiwan, R.O.C

Hui-Ming Fang
Department of Harbor and River Engineering, National Taiwan Ocean University, Keelung, Taiwan, R.O.C

Sung-Shan Hsiao
Department of Harbor and River Engineering, National Taiwan Ocean University, Center of Excellence for Ocean Engineering, Keelung, Taiwan, R.O.C., sshsiao@mail.ntou.edu.tw

Journal of Marine Science and Technology, Vol. 26, No. 4, pp. 552-561 (2018)
DOI: 10.6119/JMST.201808_26(4).0008

MORPHOLOGICAL CHARACTERISTICS OF TIDAL INLETS SUBJECT TO A SHORT TERM TYPHOON EVENT: A CASE STUDY IN LANYAN RIVER ESTUARY

Hsing-Yu Wang[1], Hui-Ming Fang[2], and Sung-Shan Hsiao[3]

Key words: sediment transport, topographic change, estuary.

ABSTRACT

This study aims to investigate different sediment particle sizes subject to transport characteristics of bed-load and suspended-load caused by nonlinear interactions of wave-tide-river in a tidal-estuary. A two-dimensional hydrodynamic coupling to a morphological model is developed to study this issue. A case study of Lanyang River estuary in Taiwan is applied and analyzed. The models are verified against field data (i.e., hydrodynamics and morphological change) collected from Lanyang River estuary during the invasion of typhoon Saola in July, 2012. Fairly good agreements are given comparing to field data. In general, the simulation indicates that suspended load could be transported toward offshore up to water depth of an order of approximately 10-15 m); it is not a major factor to affect morphological changes. The bed-load transport driven by the flood due to typhoon event is proven to be a major contribution to topographic changes in estuary. The presented results found that the erosion and siltation are both observed in the alongshore regions. In the estuary siltation of approximately 3-4 m on the north and south sides of the estuary and erosion of approximately 2-3 m are found respectively.

I. INTRODUCTION

Geomorphology studies on estuaries have mostly employed hydrodynamic field observations, topographical surveys, measurement of sediment transport and riverbed materials in conjunction with related statistical methods and neural networks to explore the relationship between related factors as well as topography evolution with changes in such regions. Analyses of mesoscale or small-scale models (such as a sedimentary dynamic model) incorporate hydrodynamic factors of sea areas (such as currents and waves) into estuary shoreline models. The hydrodynamic parameters of sea areas—acquired through basic equations describing tides, waves, and currents-can be employed in the sediment transport equation to determine the sand-transport-derived topographical changes to an estuary shoreline. This implementation has been employed in studies investigating the mechanism behind topographical changes in estuary shoreline (Ariathurai and Krone, 1976; Cole and Miles, 1983; Holly, 1984; Teision and Latteux, 1986; Christopher, 1988; Van Rijn, 1990; Ebrahim and Jean, 1995). Wave-flow interaction caused by waves and currents is an essential mechanism governing sediment movement in estuaries. Soulsby (1997) indicated that wave-flow interaction causes the suspended sediment concentration at the seabed to be 40%-100% higher than if this interaction does not occur. Waves have been discovered to not only affect sediment transport but also the force exerted by sediments at the bed and the sediment-carrying capacity of a flow. Under tidal wave transport and wave–current interaction, the shear stress on the bed plays a crucial role in inshore sediment suspension, transport, deposition and the evolution of submarine topography. The transport of sediments alters the landform, which indirectly affects the water flow. The overall hydrodynamic phenomena should be understood when performing simulations to determine the characteristics of sediment movement near estuaries. The wave effect in inshore areas cannot be neglected; however, the Boussinesq equation, which examines the high dispersion and nonlinearity of wave-wave interaction, is slightly applicable to explore this effect because of scale limitations. By contrast, the mild-slope equation has become more prevalent (Booij, 1981; Kirby, 1983; Liu, 1983). The effect of waves on the overall hydrodynamic force is incorporated into the momentum equation of shallow water waves in the form of two-dimensional (2D) or three-dimensional (3D) radiation stress (Longuet and Stewart, 1961; Longuet and Stewart, 1964; Xia

Paper submitted 05/18/18; revised 06/05/18; accepted 06/22/18. Author for correspondence: Sung-Shan Hsiao (e-mail: sshsiao@mail.ntou.edu.tw).
[1] Department of Harbor and River Engineering, National Taiwan Ocean University, Keelung, Taiwan, R.O.C.
[2] Department of Harbor and River Engineering, National Taiwan Ocean University, Keelung, Taiwan, R.O.C.
[3] Department of Harbor and River Engineering, National Taiwan Ocean University, Center of Excellence for Ocean Engineering, Keelung, Taiwan, R.O.C.

et al., 2004; Kumar et al., 2011). The use of computing methods to estimate the extent of sediment transport has been gradually extended to the calculation of complex types of wave-flow-sediment interaction (Bagnold, 1947; Bagnold and Inman, 1963; Kalkanis, 1964; Bijker, 1966; Grant and Madsen, 1979; Tanaka and Shuto, 1981; Quick, 1983). Van Rijn (1984a, 1984b, 1984c) evaluated the applicability of 3D mathematical modeling of sediments and related parameters regarding transitional flow, including sediment movement under water flow, wave-flow interaction, and other forces driven by hydrodynamic activities. The equation proposed by van Rijn is currently the most widely used equation for evaluating sediment transport. Bed shear stress under both wave and current actions is considerably higher than that under the effect of a single flow field. Through studies of wave boundary layers, Sleath (1987, 1995) discovered extreme diversity in the flow velocity structure and turbulence intensity of a boundary layer when waves were present and also investigated the flow velocity change and variation in the bed friction coefficients.

When analyzing the sediment transport mechanism for an estuary coast under the interaction between river inflow and marine processes, heterogeneous sediment transport in the river and the coupling effect between estuary and shoreline processes must be considered. Accordingly, this study accounted for different sediment particle sizes, explored the transport of bed load and suspended load sediments caused by wave-ocean and current-river inflow interaction, and investigated the characteristics of potential erosion and siltation in sea areas as well as sediment transport at estuaries. A numerical model on 2D hydrodynamics and coastal evolution was employed for simulations. The models were verified using unsteady flow data collected from rivers in Taiwan during the invasion of typhoon Saola in July 2012 and the related topographical estuary data. The overall land-sea interaction and coastal evolution were evaluated. Evolution of coasts, both river inflow and the interaction between waves and the tide, should be accounted for, particularly regarding the inshore areas, where the waves are deformed and broken by the boundary effect. Bed sediments therein are severely disturbed and then transported to downstream by longshore current, causing erosion of and accumulation along the coast. The existing literature apparently suggests that currents, waves, and river inflows are essential driving forces for the topographical evolution of estuaries. To understand the hydrodynamic forces in estuaries and the trends in topographical changes caused by wave-ocean and current-river interactions, this study developed and employed a 2D hydrodynamic and topographical evolution numerical model for simulation.

The numerical model consists of various submodels, including those describing the wave field, flow field, and topography changes; the overall calculation process is illustrated in Fig. 1. Initially, the wave module and current module are combined with data on the river inflow, tides, and broken waves to derive the radiation stress, which is used to calculate the hydrodynamic forces in the wave flow field. The calculation result is then employed in the drifting and topography change model for computing the topographical changes at the bed; these changes in turn affect the currents in the ocean current field. The related models are elaborated upon herein.

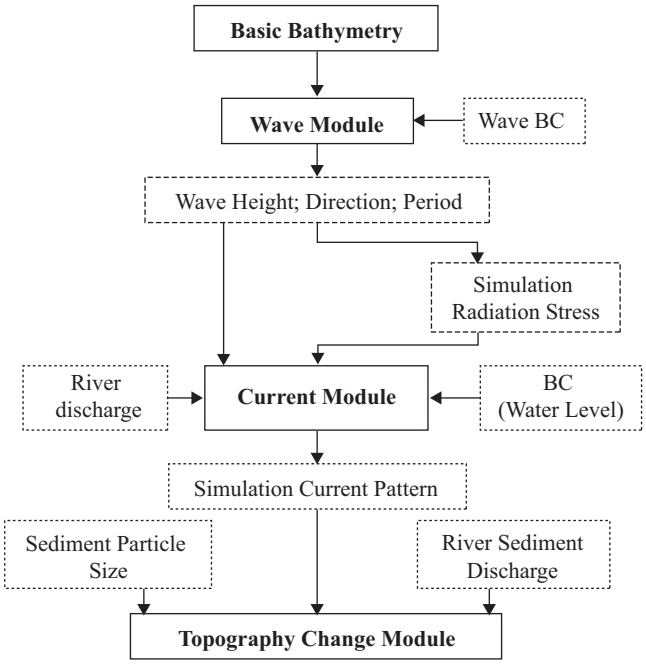

Fig. 1. Overall calculation process flowchart of the numerical model.

II. METHODOLOGY

1. Hydrodynamic Model

The governing equation of the 2D hydrodynamic model can be derived through the following process: First, the Navier-Stokes equation is simplified by assuming an incompressible fluid and hydrostatic pressure distribution. The conservation of mass and momentum equations are then acquired on the basis of a depth-integral equation and appropriate boundary conditions:

$$\frac{\partial \zeta}{\partial t}+\frac{\partial (HU)}{\partial x}+\frac{\partial (HV)}{\partial y}=0 \tag{1}$$

$$\begin{aligned}&\frac{\partial U}{\partial t}+U\frac{\partial U}{\partial x}+V\frac{\partial U}{\partial y}+g\frac{\partial \zeta}{\partial x}+g\frac{U\sqrt{U^2+V^2}}{C_z^2 H}\\&-\left(K_x\frac{\partial^2 U}{\partial x^2}+K_y\frac{\partial^2 U}{\partial y^2}\right)+\frac{1}{\rho H}\left(\frac{\partial S_{xx}}{\partial x}+\frac{\partial S_{xy}}{\partial y}\right)=0\end{aligned} \tag{2}$$

$$\begin{aligned}&\frac{\partial V}{\partial t}+U\frac{\partial V}{\partial x}+V\frac{\partial V}{\partial y}+g\frac{\partial \zeta}{\partial y}+g\frac{V\sqrt{U^2+V^2}}{C_z^2 H}\\&-\left(K_x\frac{\partial^2 U}{\partial x^2}+K_y\frac{\partial^2 U}{\partial y^2}\right)+\frac{1}{\rho H}\left(\frac{\partial S_{xy}}{\partial x}+\frac{\partial S_{yy}}{\partial y}\right)=0\end{aligned} \tag{3}$$

where ζ represents the average water level (m); $H = \zeta + h$ represents the total water depth (m); h represents the distance from the static water level to the bed (m); g is the gravitational constant (m/s^2); K_x and K_y represent the coefficients of eddy viscosity (m^2/s); U and V represent the mean flow velocity (m/s); C_z represents the Chezy coefficient; and S_{xx}, S_{xy}, S_{yx} and S_{yy} represent the components of the radiation stress caused by waves (kg/ms^2), which can be estimated using the method proposed by Longuet-Higgins and Stewart (1964):

$$\begin{bmatrix} S_{xx} & S_{xy} \\ S_{yx} & S_{yy} \end{bmatrix} = \frac{\rho g H_a^2}{g} \begin{bmatrix} n\left(1+\cos^2\theta\right)-\frac{1}{2} & \frac{n}{2}\sin 2\theta \\ \frac{n}{2}\sin 2\theta & n\left(1+\sin^2\theta\right)-\frac{1}{2} \end{bmatrix} \quad (4)$$

$$n = \frac{c_g}{c} = \frac{1}{2}\left(1+\frac{2kh}{\sinh 2kh}\right) \quad (5)$$

In these equations, c represents the wave celerity (m/s); c_g represents the group velocity (m/s); k represents the wave number (1/m); θ represents the angle of incidence of the waves (°); and H_a represents the wave height (m). The physical quantities required for the aforementioned calculation can be obtained using the wave field model. Changes in the flow field are considered to be caused by the water level gradient, the bed friction force, turbulence disturbance, and the radiation stress released after a wave breaks; the surface wind shear stress and Coriolis force are not considered here. Eqs. (1)-(3) indicate that with appropriate tidal-level boundary conditions, the alternating direction implicit method can be used to determine unknown water level changes and the average velocity of horizontal flows in the computation area. When considering changes in the intertidal zone (wet or dry condition), the relative flow velocity component is regarded to be zero with no calculation made to simulate the dry-wet boundary when the average water depth is less than 0.1 m. The bed friction coefficient and the coefficient of eddy viscosity should be determined according to the actual measurement data.

2. Wave Model

The data required to calculate radiation stress are the wave height, period, and direction, which can be obtained from various types of wave models addressing dissimilar physical problems. When both waves and tides are present, there is substantial diversity in both the spatial and temporal scales; thus, if waves and tides are considered to be on the same space-time scale, obtaining practical engineering applications for large sea areas is difficult. Accordingly, the calculation efficiency can be substantially improved if the force exerted by the wave field is regarded as steady over a certain period of time, thus ignoring instantaneous changes in wave motion. Considering refraction, diffraction, and wave breaking caused by the transmission of deep-water waves to shallow water areas, this study employed the regional coastal processes wave propagation model (RCPWAVE) for wave field calculations. The control equations are as follows:

$$\frac{1}{a}\left\{\frac{\partial^2 a}{\partial x^2}+\frac{\partial^2 a}{\partial y^2}+\frac{1}{cc_g}\left[\nabla a\cdot\nabla\left(cc_g\right)\right]\right\}+k^2-\left|\nabla s\right|^2=0 \quad (6)$$

$$\frac{\partial}{\partial x}\left(a^2 cc_g\left|\nabla s\right|\cos\theta\right)-\frac{\partial}{\partial y}\left(a^2 cc_g\left|\nabla s\right|\sin\theta\right)=0 \quad (7)$$

$$\frac{\partial}{\partial x}\left(\left|\nabla s\right|\sin\theta\right)-\frac{\partial}{\partial y}\left(\left|\nabla s\right|\cos\theta\right)=0 \quad (8)$$

where a represents the wave amplitude (m) and S represents the phase function. RCPWAVE solves the mild-slope equation of the parabolic type in a stable and fast manner with minimum computational calculation; hence, the model is reasonably applicable for making engineering application calculations for large sea areas. The wave-breaking index $H_a/h = 0.78$ is used for estimation of wave breaking. In the calculation of breaking waves, the flow velocity in the breaker zone is calculated on the basis of the longshore currents theory of Longuet-Higgins and Stewart (1964). The wave model generally employs water level fluctuation due to tidal changes as the water depth input condition for the calculation, and the calculated wave height, period, and direction are further used in the wave radiation stress calculation.

3. Fine Sediment Transport Model

The calculation of bed elevation changes is determined by the net change in sediment transport (total load). The mass conservation equation for bed elevation changes is as follows:

$$\frac{\partial z}{\partial t}=\frac{1}{1-\lambda}\left(\frac{\partial Q_x}{\partial x}+\frac{\partial Q_y}{\partial y}+q_D-q_E\right) \quad (9)$$

where Z represents the bed elevation (m); λ represents the porosity of the bed material, which is generally 0.35-0.41, but the optimal value of which should be based on calibration; Q_x and Q_y respectively represent the longshore and offshore unit width sediment transport rate associated with the bed load (m^2/s); and q_D and q_E respectively represent the accumulation related to the suspended load and the sediment transport rate of resuspension (m/s).

4. Bed Load Transport Model

Sediment transport of the bed load was calculated using the equation proposed by Van Rijn (1984a, 1984b):

$$\begin{cases} Q_x = Q_{bx} + Q_{sx} \\ Q_y = Q_{by} + Q_{sy} \end{cases} \quad (10)$$

where Q_{bx} and Q_{sx} represent the longshore sediment transport of the bed load and the suspended load, respectively, and Q_{by} and Q_{sy} represent the offshore sediment transport of the bed load and the suspended load. The calculation of each equation is performed as follows:

$$\begin{cases} Q_{bx} = Q_b \dfrac{U}{\sqrt{U^2+V^2}} \\ Q_{sx} = C_a FUh \end{cases} \tag{11}$$

$$\begin{cases} Q_{by} = Q_b \dfrac{V}{\sqrt{U^2+V^2}} \\ Q_{sy} = C_a FVh \end{cases} \tag{12}$$

Q_b and C_a can be calculated as follows:

$$Q_b = 0.053\left[(s-1)g\right]^{0.5} D_{50}^{1.5} D_*^{-0.3} T^{2.1} \tag{13}$$

$$C_a = 0.015 \frac{D_{50}}{a} \frac{T^{1.5}}{D_*^{0.3}} \tag{14}$$

T and $D_{*(i)}$ be calculated through:

$$D_* = \left[(s-1)g\upsilon^{-2}\right]^{1/3} D_{50} \tag{15}$$

$$F = \frac{(a/h)^{z'} - (a/h)^{1.2}}{(1-a/h)^{z'}(1.2-z')} \tag{16}$$

$$T = \frac{\tau_{b,c}^{'} - \tau_{b,cr}}{\tau_{b,cr}} \tag{17}$$

$$\tau_{b,c}^{'} = \rho g \left(\frac{\sqrt{U^2+V^2}}{C'} \right)^2 \tag{18}$$

$$\tau_{b,cr}^{'} = (\rho_s - \rho) g D_{50} \theta_{cr} \tag{19}$$

In these equations, s represents the silt ratio; D_* represents the non-dimensional silt particle size; D_{50} represents the median diameter of the bed material; F is the shape factor; z' represents the suspension constant; a represents the bed surface roughness; υ represents the viscosity coefficient of the fluid motion (minimum is set to 0.01 h); T represents the non-dimensional shear stress (when T is less than or equal to zero, the sediment transport rate of the bed load is zero); $\tau_{b,cr}$ represents the critical shear stress of the bed; $\tau'_{b,cr}$ represents the bed shear stress; ρ_s represents the silt density; θ_{cr} is the Shields mobility parameter; and C' is the grain-related Chezy coefficient of bottom friction.

5. Cohesive Sediment Transport Model

Suspended sediment movement is derived from solving the diffusion equation of the sediment transport concentration. The control equation is

$$\begin{aligned} &\frac{\partial(HB)}{\partial t} + U\frac{\partial(HB)}{\partial x} + V\frac{\partial(HB)}{\partial y} \\ &= \frac{\partial}{\partial x}\left(HD_x \frac{\partial B}{\partial x}\right) + \frac{\partial}{\partial x}\left(HD_y \frac{\partial B}{\partial y}\right) + S* \end{aligned} \tag{20}$$

where B represents the average sediment concentration (mg/L); D_x and D_y represent the diffusion coefficients in the horizontal directions (m^2/s); and S* represents the concentration change term:

$$S* = QB_{river} - Q_D + Q_E \tag{21}$$

B_{river} represents the average concentration of sediment transported by river inflow; Q represents the discharge of river inflow per unit area (cms/m^2); Q_D represents the deposition rate (mg·m/sL); and Q_E represents the erosion rate (mg · m/sL). The shear stress on the bed, an essential factor affecting deposition or resuspension of suspended sediment, can be estimated according to the law of friction on the basis of boundary layer theory. The settling velocity (W_s) is estimated using the deposition law proposed by Krone (1962):

$$W_s = K_1 B^{4/3} \tag{22}$$

where $K_1 = 0.0012$ is the suggested value.

III. FINE SEDIMENT TRANSPORT AND MORPHOLOGICAL CHANGE DUE TO TYPHOON SAOLA

1. Modeling Procedure and Validation

The model was developed by examining the environmental background data, selecting the range to be simulated, and calibrating the tidal model. Field investigation was performed, and data were collected to calculate the required environmental background data using the integrated model; these data included such as ocean phenomena, particle size of sediment on the bed, the characteristics of sediment transport by flood and other water bodies, and water depth. This study collected topographic data of estuaries before and after the invasion of typhoon Saola in July 2012 to verify the trend in topographic changes estimated by the model. Table 1 lists the configuration settings of the hydrodynamic model. The model was verified as follows. Boundary conditions were set and parameter calibration was performed on the basis of the current data measured during April and September 2012. The calibrated model parameters were then used to simulate the topographic changes and sediment transport in the Lanyang estuary during flood season of typhoon Saola,

Table 1. Calculation conditions for hydrodynamic model calibration.

Item	Hydrodynamic model
Area	24 km × 17 km
Grid size	50 m × 50 m
Number of grid points	551 × 391
Coordinate of the origin (TWD97)	(325630, 2746180)
Angle of deviation (counterclockwise from the north)	78°
time step size	1.5 s
Coefficient of eddy viscosity	K_x = 500 (m^2/s) K_y = 100 (m^2/s)
Chezy coefficient	14.0

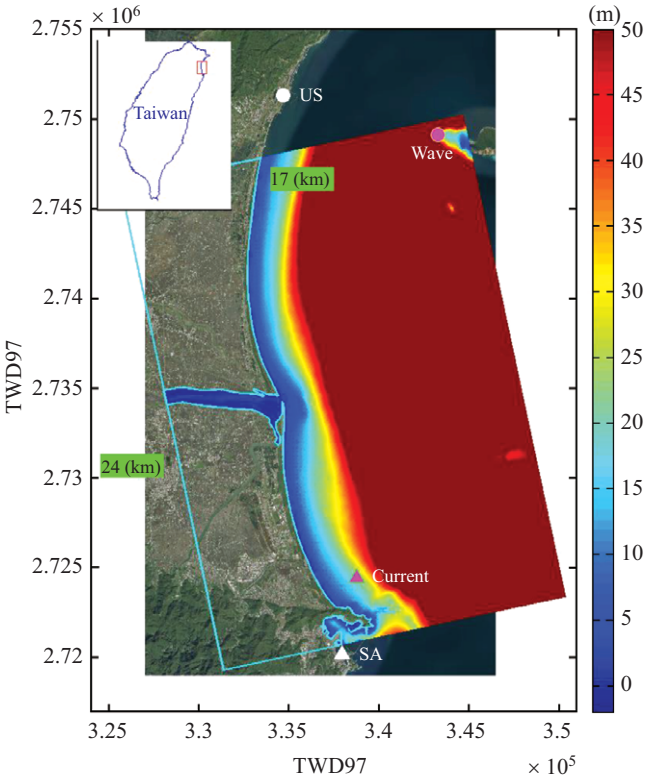

Fig. 2. Geographic location and computed domain in the Lanyang River estuary. US and SA: tidal gauge; Current and Wave: tidal current and wave buoy stations in 2012.

with the results compared with the measured topographic data. Fig. 2 displays the calculation range of the model and the applied topographical data; the calculation ranged from south of Wushih Fishing Port in the north to Suao Bay in the south and was bounded by Lanyang Bridge in the west. The calculation range encompassed a wave and tide measuring station and the Guishandao buoy. The topography data employed by the model comprised the data measured in April 2012 and 200 m water depth data from the National Science Council.

The hourly boundary conditions comprised the Wushih Fishing Port tide level, Suao Bay tide level, flow velocity and sediment transport in the Lanyang estuary, significant wave height, significant wave period, and wave direction measured by the Guishandao buoy (Fig. 3). The tide level data were employed as the boundary conditions on the north and south sides of the area; the river discharge and sediment transport were used as the boundary conditions for the river inflow; and finally, the Guishandao buoy data were employed as the incident conditions of the waves in the open ocean. Fig. 4 compares the model simulation results with the actual current measurement. The calculated inshore flow velocity, offshore flow velocity, flow direction, and changes in water level were all highly consistent with the measured data. The currents simulated by the model generally flowed parallel to the coastline. Specifically, the current flowed from the south-

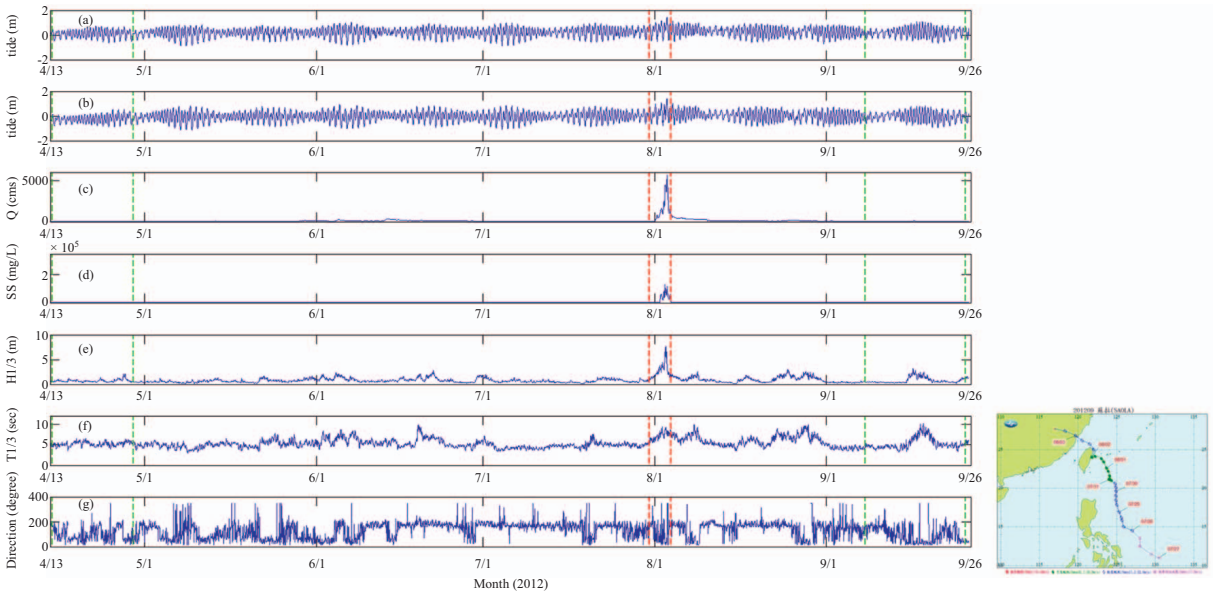

Fig. 3. Hourly boundary conditions applied in the computation. (a) US tide; (b) SA tide; (c)River discharge; (d) Fine sediment concentration; (e) $H_{1/3}$; (f) $T_{1/3}$; (g) Wave direction. Green line: Onsite observation period (2012/4/14-4/28; 2012/9/7-9/25); Red line: Typhoon SAOLA (2012/7/30-8/3).

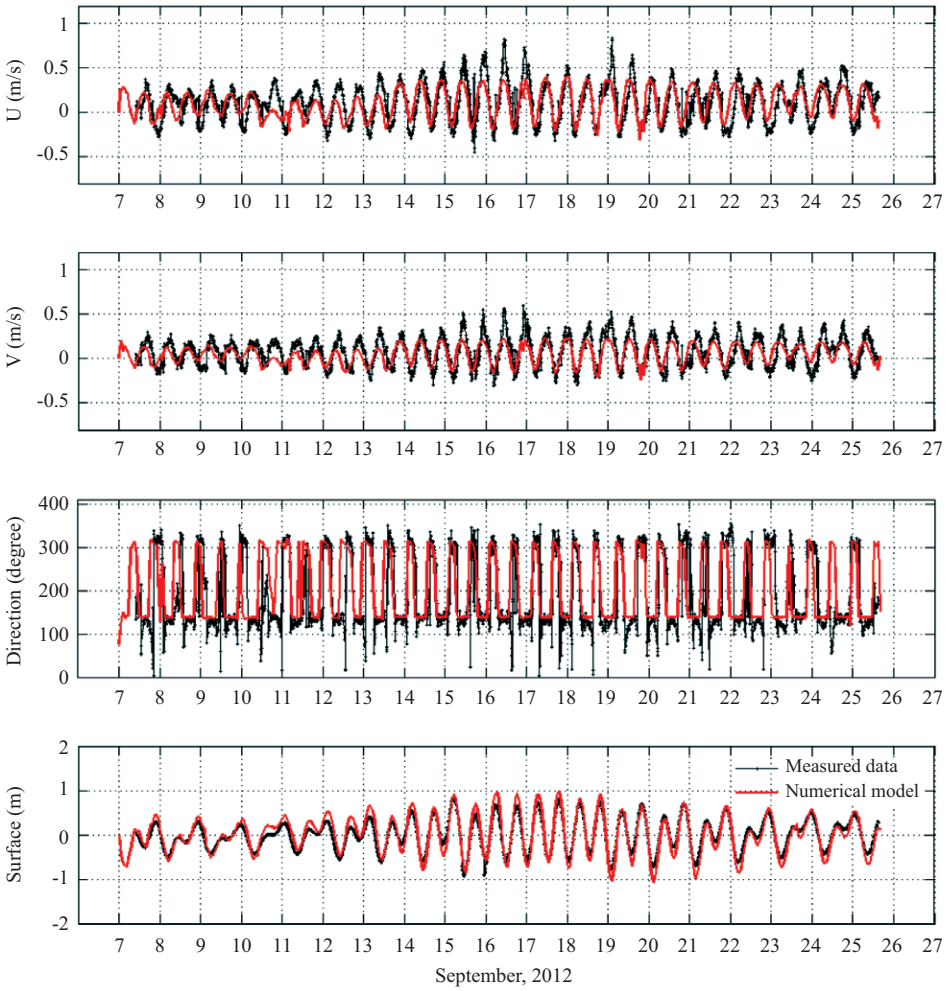

Fig. 4. Comparison between field data and numerical model.

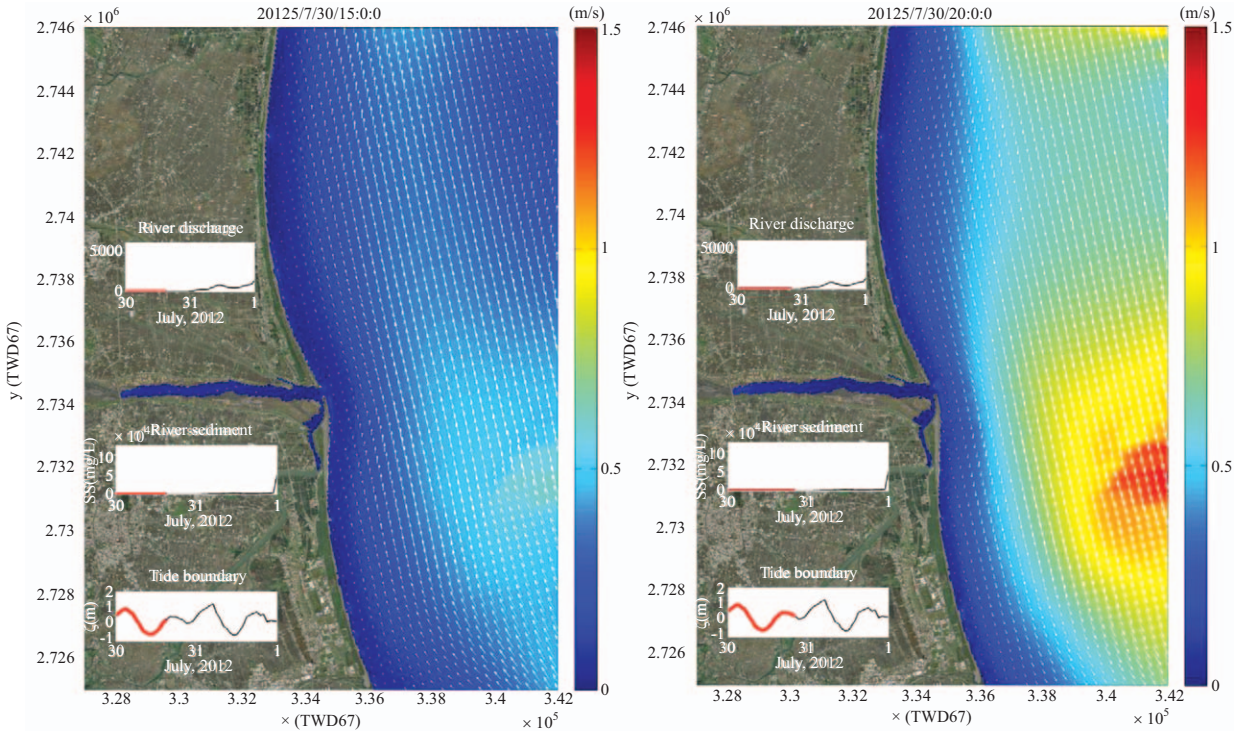

Fig. 5. Computed flow field and direction during flood (left) and ebb (right) tides in the Lanyang estuary.

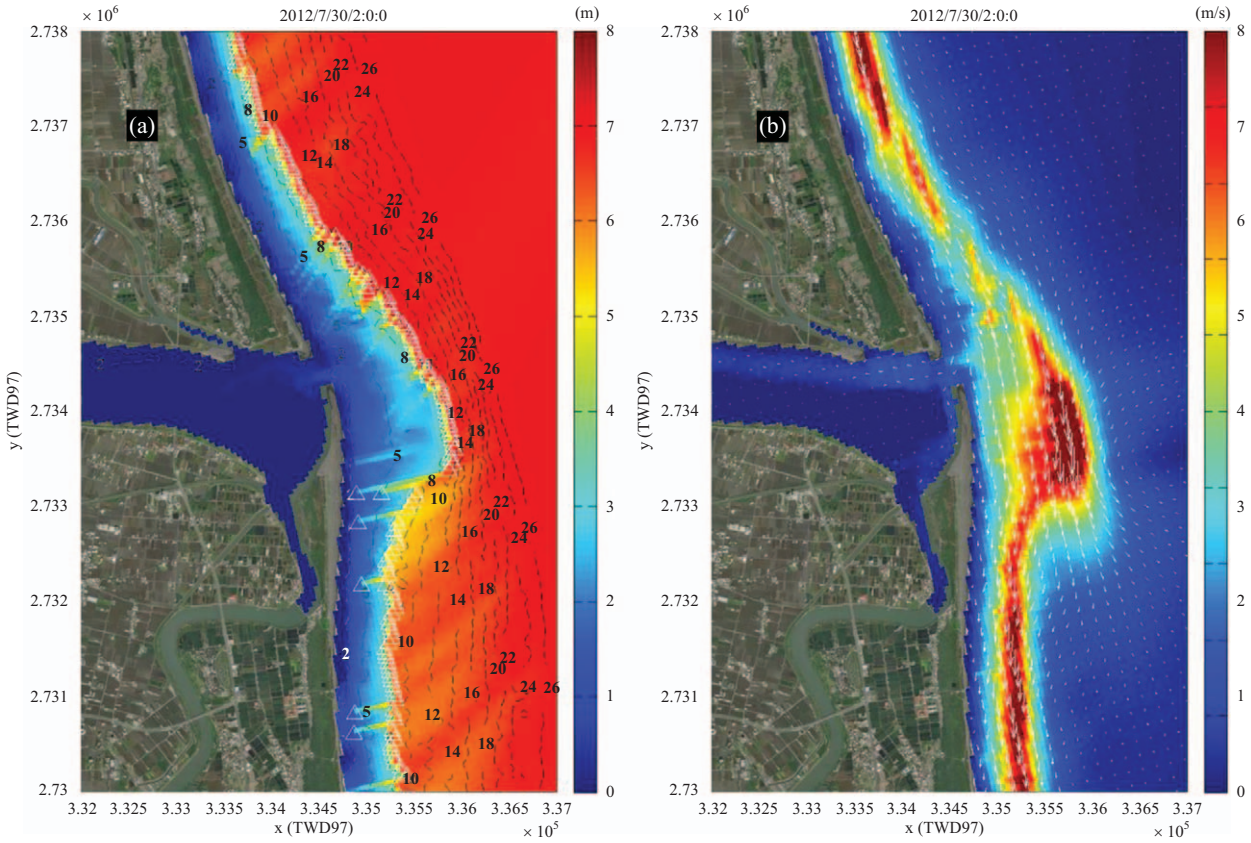

Fig. 6. Computed wave height distribution and wave breaking locations of typhoon waves (H = 7.74 m; T = 9.2s; NE direction) (left) and corresponding Longshore current speed (right) in the Lanyang estuary.

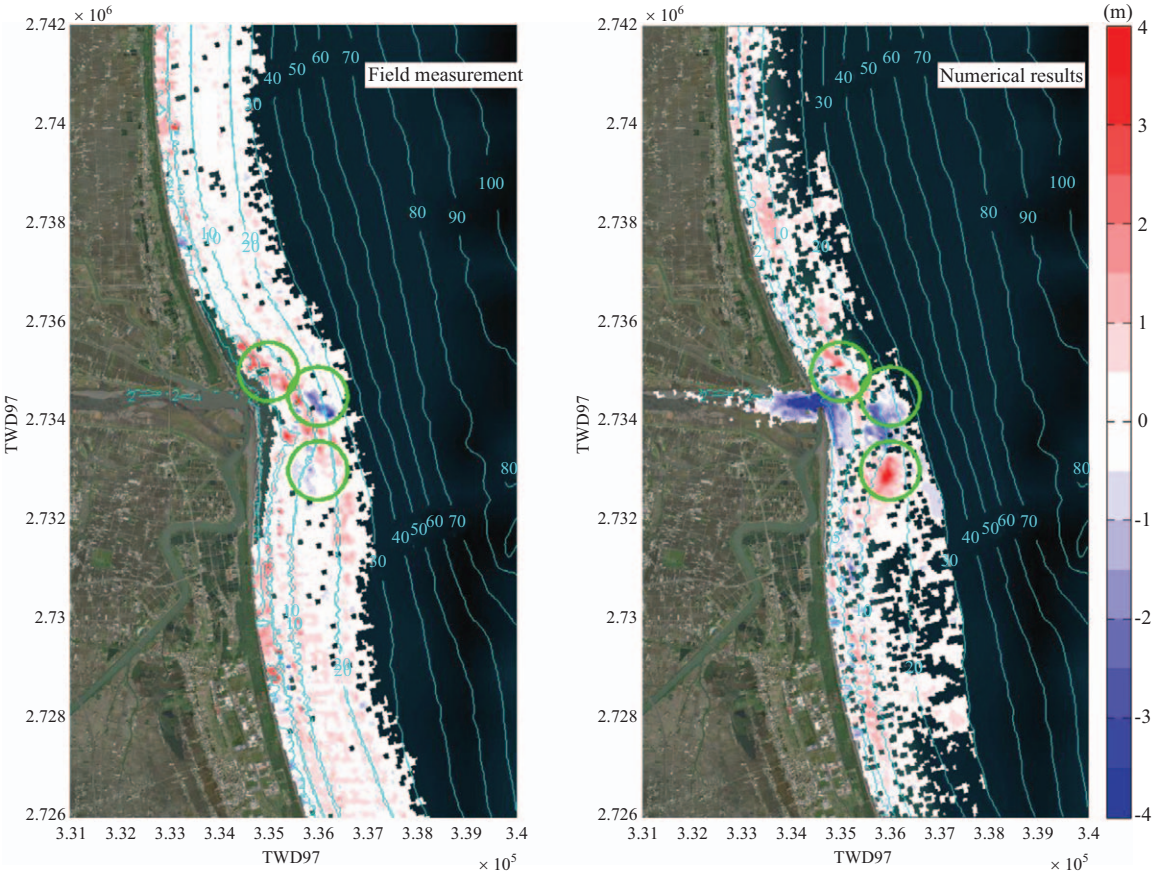

Fig. 7. Comparison between measurement bathymetry change and numerical models.

east to the northwest during flood tides and from the northwest to the southeast during ebb tides. The results, in accordance with the actual situation, indicate that the model successfully reproduce the characteristics of the current in the sea area adjacent to the Lanyang estuary. After the boundary conditions and related parameters adopted by the hydrodynamic model were determined, the model was employed to calculate the hydrodynamic and sediment transport characteristics in the Lanyang estuary during the invasion of typhoon Saola.

2. Hydrodynamic Characteristics at the Coast

The results of the hydrodynamic simulation are first explained. Fig. 5 presents the spatial distribution of flow velocities during flood tides and ebb tides before the advent of the typhoon Saola. As previously stated, the currents moved from the southeast to the northwest during flood tides and from the northwest to the southeast during ebb tides. The flow velocity of the Lanyang stream was relatively low compared with the ocean current at this time, and the stream mostly entered the sea along the main channel. Fig. 6 shows the characteristics of the coastal wave currents entering the estuary of the Lanyang stream before the advent of the Typhoon Saola. Incident waves from the northeast direction broke at approximately 2 m in depth, and the energy released after the wave breaking induced longshore currents that traveled from the northwest to the southeast.

3. Fine Sediment Transport Behavior

Fig. 7 displays a topographic map of the erosion-siltation phenomenon at the Lanyang estuary coast from April to September in 2012, which was used as verification data for the simulation of topographic changes. A simulation uses the topography properties method to a comparison between measurement bathymetry change and numerical models. Even though the simulated sea area on the south side of the estuary was determined to be wider than the actual area, both the model calculation data and measured data indicate siltation of approximately 3-4 m on the north and south sides of the estuary and erosion of approximately 2-3 m in the open area of the estuary. In the coastal area, siltation and erosion were both discovered, but siltation was the principal phenomenon. Overall, the two data sets are moderately consistent, both qualitatively and quantitatively. Therefore, the proposed numerical model was verified to be capable of reasonably simulating the drifting mechanism and topographic changes in the Lanyang estuary.

4. Morphological Change Behavior

After verifying the proposed models, this study employed the flooding event caused by typhoon Saola in July 2012 as a

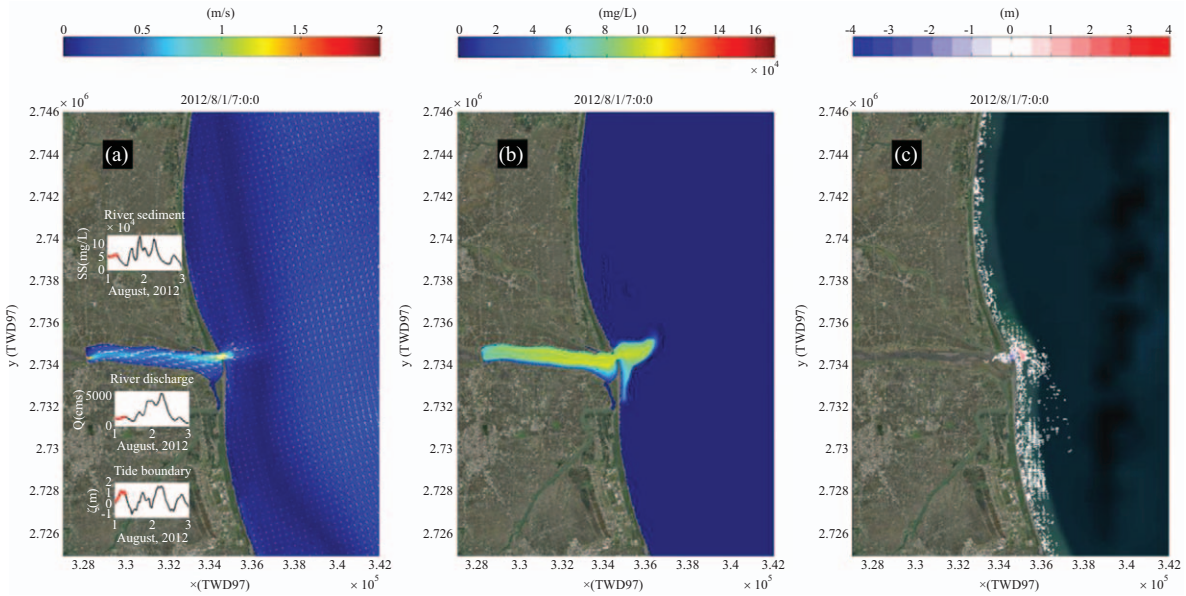

Fig. 8. (a)Flow velocity, (b)fine sediment and (c)bathymetry change before the flood period of typhoon Saola.

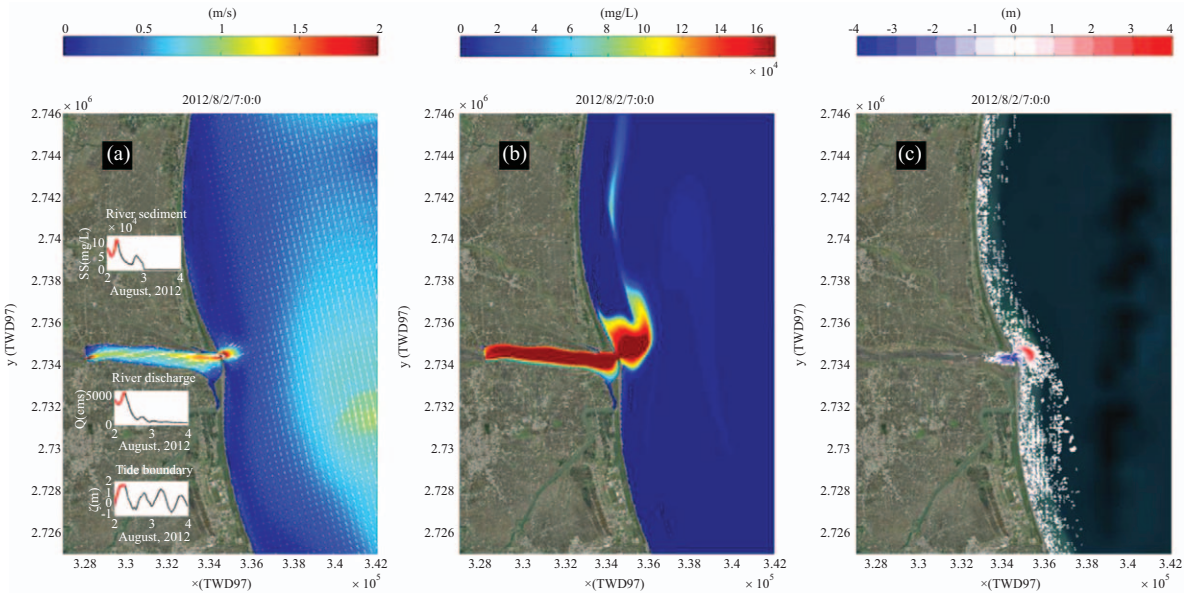

Fig. 9. (a) Flow velocity, (b) fine sediment and (c) bathymetry change at the flood period of typhoon Saola.

simulation subject. The bed load distribution employed by the model was derived from actual measurement conducted in this study. The distribution was assumed to be even. The particle size (d50) of the bed load was assumed to be 0.3 mm. Figs. 8 and 9 present a series of maps illustrating the spatial distribution of flow velocity, suspended sediment, and topographic erosion and siltation in the Lanyang estuary during the major periods of flooding—namely, before during, and after the flood peak. The results revealed that before the flood occurred, erosion and siltation at the coastal area were caused by the longshore currents created by breaking waves; by contrast, no erosion-siltation phenomenon occurred in the estuary. As the flood began, the level of the river rose considerably and then flowed onto the floodplains on either side of the river; additionally, the flow velocity in the estuary increased. The rising water level led to the submergence of sandbars in the Lanyang River channel; the amount of suspended sediment in the river channel gradually increased, and this sediment began to be transported to the estuary area; and finally, erosion and siltation began to occur in the estuary area due to the swinging phenomenon of the sand tongue caused by repetitive tidal movements. After the flood peak had passed through the upstream boundary during the flood peak period,

water flooded the riverbanks on both sides. The maximum flow velocity in the estuary was 2.0 m/s or higher. At this time, the water level and jet flows in the estuary pushed the bed load in the channel into the open ocean under powerful flow velocity, resulting in clear estuary erosion and deposition in the outer sea. After the flood had receded, the flood peak passed through the estuary and the water level and jet flows in the estuary decreased as the flood weakened; deposition in the estuary also slowed down.

This study simulated flow field changes during the flood caused by typhoon Saola in July 2012. Over the simulated area, the tidal currents in the open ocean still changed according to the tide level; the currents moved from the southeast to the northwest during flood tides and from the northwest to the southeast during ebb tides. These currents became jet flows as the flood approached the estuary. The jet flows, exhibiting a turbulent pattern due to tidal currents, mostly flowed outward in the direction ENE to N, with their central axis slightly offset to the left bank of the estuary.

High sediment concentration and discharge resulted from the flood period during the typhoon and caused a substantial change in the estuary's topography. The central channel in the Lanyang estuary was scoured deeply, whereas the silt flushed down by the flood was mainly deposited at water depths of 5-10 m, with a thickness of deposition of 3-4 m. The siltation area on the south side of the simulated estuary was wider than the actual measured siltation area. However, the main characteristics determined by the model, such as the water depth and deposition thickness of river siltation, were consistent with the actual measurements. The numerical model is thus adequate for simulation of the drifting mechanism and topographic evolution of the Lanyang estuary.

IV. CONCLUSION

The coastal topographic features of an estuary are formed by interactions between the sediment transport in rivers and the related processes of tides, waves, currents in sea areas. The coupling effect of river inflow and tides-waves-currents is considered in this model. With the Lanyang estuary as a research subject, this study simulated the coastal topographic features of the estuary under various inflow conditions. We use the estuary topography data of an unsteady flow of the river during the invasion of typhoon Saola in July, 2012. The simulation indicated that topographic changes to the estuary were mainly due to bed-load transport driven by an extreme increase in the river velocity, which was the result of floods caused by the typhoon. The validated model can be used to simulate the effect of sediment transport in the Lanyang estuary on the adjacent coasts. In addition to attempting to understand the major sediment transport mechanism and its impact within the studied area, subsequent studies can employ the flow velocity with suspended sediment concentration during different return periods for scenario simulation. Coastal protection measures can be implemented according to the analysis of trends in the targeted area under various circumstances.

REFERENCES

Ariathurai, R. and R. B. Krone (1976). Mathematical modeling of sediment transport in estuaries, in Estuarine Processes, Vol. II, edited by M. Wiley, 98-106, Elsevier, New York.

Bagnold, R. A. (1947). Sand movement by waves, some small scale experiments with sand of very low density. J. Inst. Civil Eng. 121.

Bagnold, R. A. and D. L. Inman (1963). Beach and nearshore processen, in the sea by M. N. Hill(ed), Interscience Publisher 3, 507-553.

Bijker, E. W. (1966). The increase of bed shear in a current due to wave motion. Proceedings of the 10th International Conference on Coastal Engineering, ASCE, 746-765.

Booij, N. (1981). Gravity waves on water with non-uniform depth and current. Delft University of Technology, Report 81.

Cole, P. and G. V. Miles (1983). Two-dimensional model of mud transport. Journal of Hydraulic Engineering 109(1), 1-12.

Ebersole, B. A., M. A. Cialone and M. D. Prater (1986). RCPWAVE—a linear wave propagation model for engineering use. Regional Processes Numerical Modelling System, Report No 1, Department of the US Army.

Grant, W. D. and O. S. Madsen (1979). Combined wave and current interaction. Journal of Geophysical Research 84(C4), 1797-1808.

Kirby, J. T. (1983). A parabolic equation for the combined refraction-diffraction of Stokes waves by mildly varying topography. Journal of Fluid Mechanics 136, 453-466.

Kumar, N., G. Voulgaris and J. C. Warner (2011). Implementation and modification of a three-dimensional radiation stress formulation for surf zone and rip-current applications. Coastal Engineering 58, 1097-1117.

Kalkanis, G. (1964). Transportation of turbulence at bed material due to wave action. Tch. Mem. U. S. Coastal Eng., Res. Center 2, 38.

Liu, P. L.-F. and T. K. Tsay (1983). On weak refraction of water waves. Journal of Fluid Mechanics 131, 59-71.

Longuet-Higgins, M. S. and R. W. Stewart (1961). The changes in amplitude of short gravity waves on steady non-uniform currents. Journal of Fluid Mechanics 10, 529-549.

Longuet-Higgins, M. S. and R. W. Stewart (1964). Radiation in water waves: a physical discussion with applications. Deep-sea Research 11, 529-563.

Sleath, J. F. A. (1987). Turbulent oscillatory flow over rough beds. J. Fluid Mech. 182, 369-409.

Sleath, J. F. A. (1995). Coastal bottom boundary layers. Appl. Mech. Rev. 48(9), 589-600.

Tanaka, H. and N. Shuto (1981). Friction coefficient for a wave-current coexistent system. Coastal Engineering Journal 24, 105-128.

Van Rijn, L. C. (1984a). Sediment transport, Part I: Bed load transport. Journal of Hydraulic Rngineering 110(10), 1431-1456.

Van Rijn, L. C. (1984b). Sediment transport, Part II: Suspended load transport. Journal of Hydraulic Rngineering 110(10), 1613-1641.

Van Rijn, L. C. (1984c). Sediment transport, Part III: Bed forms and alluvial roughness. Journal of Hydraulic Rngineering 110(12), 1733-1754.

Van Rijn, L. C. (1990). Principles of Fluid Flow and Surface Waves in Rivers, Estuaries, Seas and Oceans. Aqua Publications, P. O. Box 9896, Amsterdam, The Netherlands.

Xia, H., Z. Xia and L. Zhu (2004). Vertical variation in radiation stress and wave-induced current. Coastal Engineering 51, 309-321.